

Segregation and trapping of erbium during silicon molecular beam epitaxy

R. Serna,^{a)} M. Lohmeier, P. M. Zagwijn, E. Vlieg, and A. Polman
FOM-Institute for Atomic and Molecular Physics, Kruislaan 407, 1098 SJ Amsterdam,
The Netherlands

(Received 21 November 1994; accepted for publication 17 December 1994)

Erbium surface segregation is observed during growth of Er-doped Si by molecular beam epitaxy on Si(100) at 600 °C. Once a critical Er surface areal density of 2×10^{14} Er/cm² is reached, enhanced Er trapping is observed, possibly due to the formation of silicide precipitates. Er segregation on Si(100) is fully avoided when growth is performed in an oxygen background pressure of $\sim 10^{-10}$ mbar, due to the formation of Er-O complexes. No Er segregation is observed on Si(111), which is attributed to the formation of epitaxial Er₃Si₅ precipitates. © 1995 American Institute of Physics.

A number of papers have been published lately on the optical doping of silicon with erbium. The aim is to obtain light emitting devices using the luminescence of the Er³⁺ ion at 1.5 μm, a standard communication wavelength. In order to obtain efficient devices Er concentrations of at least 10¹⁸/cm³ are needed.¹ As the use of near-equilibrium crystal growth methods limits the rare-earth incorporation to the maximum solid solubility, nonequilibrium techniques have been used, e.g., ion implantation either directly into crystalline Si,²⁻⁷ or during molecular beam epitaxy (MBE).⁸ Incorporation of Er by ion implantation induces amorphization of the Si crystal. During solid phase epitaxy (SPE) of the Er-doped amorphous Si, segregation and trapping takes place, and up to 10²⁰ Er/cm³ can be incorporated in the crystalline Si.^{5,6} MBE coevaporation of Si and Er offers the opportunity to grow in a direct way thick Er-doped layers. There are a few reports on Er doping by MBE,⁹⁻¹¹ however the kinetics of incorporation and its limiting factors have not been studied in detail. In this letter, it will be shown that strong Er surface segregation occurs during MBE on Si(100), which is avoided when introducing an oxygen background pressure during growth. No segregation is observed on Si(111).

Erbium-doped epitaxial Si layers were grown in a MBE apparatus utilizing an electron beam evaporator for Si and a Knudsen cell for coevaporation of Er. The Si flux was 1.5×10^{14} atoms/cm² s in all cases. The Er flux was varied in the $3-14 \times 10^{10}$ atoms/cm² s range by regulating the Knudsen cell temperature between 1030 and 1100 °C. Float zone Si(100) or Si(111) crystals were used as substrates. The native oxide on the Si surface was removed by briefly heating the sample to 1100 °C in ultrahigh vacuum (base pressure 3×10^{-11} mbar). After this treatment the surface exhibited a clear 2×1 [Si(100)] or 7×7 [Si(111)] reflection high-energy electron diffraction pattern. A 20 nm thick Si buffer layer was first grown before opening the Er Knudsen cell to ensure good initial epitaxy. Subsequently, codeposition of Er and Si was performed, resulting in a ≈ 100 nm thick Er-doped film. Typical growth pressures during deposition were 6×10^{-11} mbar, and the substrate temperature was kept at 600 °C. In order to study the role of oxygen in

the Er-doping, oxygen was introduced in the MBE chamber through a needle valve. The Er concentration depth profiles, layer thickness, and Si crystal quality were measured with Rutherford backscattering spectrometry (RBS)/channeling using 2 MeV He. A backscattering angle of 100° was used to give a depth resolution better than 10 nm.

Figure 1 shows RBS channeling and random spectra for a sample grown with an Er flux of 3.1×10^{10} atoms/cm² s. The channeling minimum yield in the as-grown layer is $\chi_{\min} < 3\%$, indicating good crystal quality. A clear surface peak is observed for the Er signal, which accounts for 78% of the total amount of deposited Er. These data show that strong surface segregation takes place during growth. The profile shows a monotonic increase of the Er bulk concentration from the substrate interface towards the surface up to 4×10^{18} Er/cm³. The profiles for the channeling and random configurations overlap, indicating that Er is not in Si lattice positions, nor in tetrahedral interstitial sites.

To have a further insight in the kinetics of the segregation process, Fig. 2(a) shows the Er profiles from RBS for the 100 nm thick film from Fig. 1, and for a thinner film

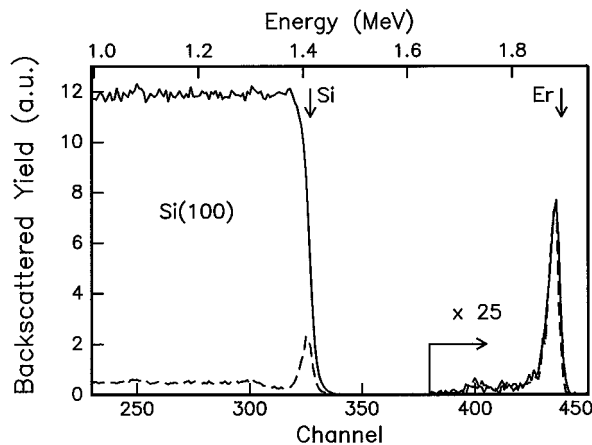


FIG. 1. RBS random (solid line) and channeling (dashed line) spectra for an Er-doped MBE film grown on Si(100) at 600 °C. Er and Si fluxes were 3.1×10^{10} and 1.5×10^{14} atoms/cm² s, respectively. The Er signal is magnified by a factor of 25. The arrows indicate the surface channels for Si and Er.

^{a)}Present address: Instituto de Optica, CSIC, Serrano 121, 28006 Madrid, Spain.

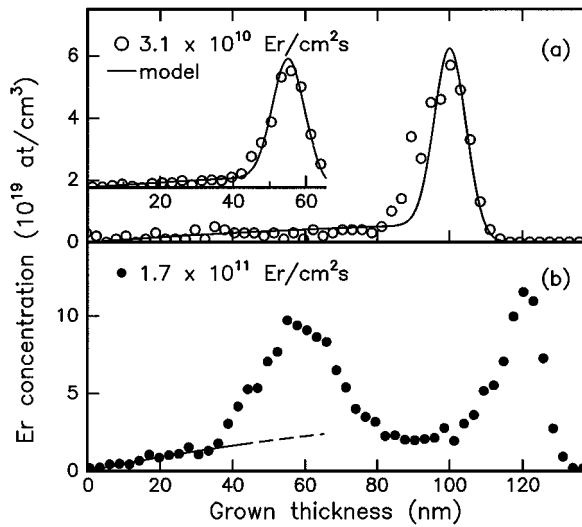


FIG. 2. Er concentration as a function of thickness for MBE films on Si(100) at 600 °C. The Er flux was 3.1×10^{10} atoms/cm² s (a), or 1.7×10^{11} /cm² s (b). The data of the thin sample in (a) are offset vertically to facilitate comparison. In this figure the horizontal scale has been converted to grown thickness of the Si film. Therefore, the Er surface peaks appear at different thickness. The full lines are the calculated profiles according to a kinetic two-dimensional growth and segregation model.

(~55 nm) grown under the same conditions. The profile of the thin film is identical to the thick one in the first 40 nm. As the growth is stopped in an earlier stage the surface peak is smaller. The Er profiles of Fig. 2(a) can be very well described by a kinetic two-dimensional growth and surface segregation model. This model assumes that there is a small incorporation probability (α) of Er for each monolayer of growing crystal, due to the low solubility of Er in Si. The Er can escape from being incorporated in the crystal via a “step-climbing process” at the surface during growth. Assuming no desorption takes place, the Er bulk concentration N_b as a function of the distance z from the Si substrate interface is then given by:¹²

$$N_b(z) = \frac{F_d}{v_g} (1 - e^{-z/\Delta}), \quad (1)$$

where F_d is the dopant flux, and v_g is the growth rate. The parameter $\Delta = h/\alpha$ is the characteristic film thickness required to reach steady-state doping, with h the step height. At each point during growth the surface areal density of segregated Er, N_s , is then proportional to the concentration trapped in the crystal

$$N_s(z) = N_b(z) \frac{h}{\alpha}. \quad (2)$$

The higher the surface step or the lower the incorporation probability, the higher will be the density of segregated Er. In Fig. 2(a) the calculation performed with this model is overlaid for the two samples. The data are convoluted with a depth resolution of 8 nm. Good agreement with the experimental data is obtained in both cases for an incorporation probability of $\alpha = 1.5 \times 10^{-3}$.

Figure 2(b) shows the Er profile for a sample grown with a higher Er flux, 1.7×10^{11} atoms/cm² s. The model de-

scribed above fits these data with the same value for α [drawn line in Fig. 2(b)], until a sharp increase in the bulk concentration takes place at a thickness of about 35 nm. At this point the Er concentration suddenly increases, from $\sim 2 \times 10^{19}$ to 1×10^{20} /cm³. After this maximum the Er concentration decreases again and finally an Er peak is observed at the surface. Good channeling is achieved for this film ($\chi_{\min} = 3\%$), indicating that the Si crystal quality is still good. A similar behavior has been observed for other Er fluxes higher than 7×10^{10} atoms/cm² s. A possible explanation of this incorporation instability is that erbium silicide precipitates are formed when the Er surface areal density reaches a critical value. A large fraction of the segregated Er is then suddenly incorporated in the crystal, and therefore the amount of Er at the surface decreases. Subsequently, the segregation process continues, and the Er concentration at the surface increases again. This model implies that when thicker films are grown, or higher Er fluxes are used, an oscillatory change in the growth mode will be observed, resulting in a depth modulation of the precipitates density. Figure 2(b) shows that the maximum Er concentration which can be incorporated by MBE without precipitation at 600 °C is 2×10^{19} Er/cm³. The corresponding areal density [from Eq. (2)] is $\sim 2 \times 10^{14}$ Er/cm² (a coverage of about 30%). This is the threshold areal density above which the instability takes place. Such a high surface Er coverage is not achieved for the low Er flux, in which case the incorporation remains stable. The formation of silicide precipitates has been observed earlier in Er-doped films grown by MBE.^{9,10} However, our data indicate that these precipitation phenomena during MBE have a kinetic rather than a pure thermodynamic origin.^{9,10}

It is interesting to note the analogy with Er incorporation by ion implantation and SPE at 600 °C. During SPE segregation of the Er is also observed, the incorporation also becomes unstable, though for larger concentrations (1.2×10^{20} Er/cm³), and is accompanied by the formation of crystal twins.⁵ In the MBE case the Er which is not incorporated in the crystal segregates towards a free surface, whereas in the case of SPE the excess Er is incorporated in the amorphous phase and distributed in a ~ 3 nm thick segregation spike,⁶ thus allowing a higher segregated Er density before precipitation takes place.

Oxygen has a large influence on the Er segregation behavior during MBE. Figure 3 shows the Er depth profile after MBE on Si(100) in an oxygen ambient of 4×10^{-10} mbar, and the profile after MBE without oxygen at the same Si and Er rates [Fig. 2(a)]. The area under both curves is the same, and evaluates to a total areal density 1.0×10^{14} Er/cm². The channeling minimum yield for the film grown in an oxygen background is as good as that obtained for the films grown without oxygen ($\chi_{\min} < 3\%$). From the profile it can be seen that after a transient (≈ 50 nm), during which the Er concentration gradually increases, a final steady-state concentration of 1.5×10^{19} /cm³ is reached.

It has been shown that oxygen can play an important role in the optical activation of Er in Si.^{3,4,7,11,13} The important reduction in the segregation of Er induced by oxygen during MBE growth is an additional advantage of the codoping with

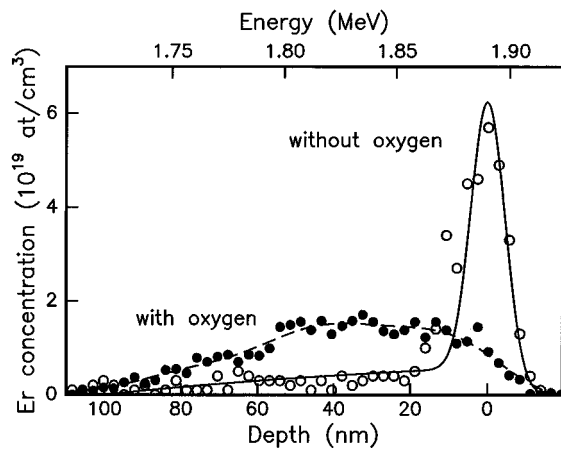


FIG. 3. Er concentration depth profile of a MBE film grown on Si(100) at 600 °C, at an oxygen background pressure of 4×10^{-10} mbar. The Er flux was 3.1×10^{10} /cm² s (full circles). The Er profile of the corresponding film grown without oxygen (background pressure $< 6 \times 10^{-11}$ mbar) is included for reference (open circles). The dashed line is a guide for the eye.

oxygen. The fact that the dopant profile is very sensitive to oxygen contamination may explain why Er segregation has not been reported previously. The increased Er incorporation in the presence of oxygen may have two different origins. First, it may be that O influences the growth for example by decreasing the adatom mobility, or changing the energy barrier to climb steps.¹⁴ Second, O may react with Er at the Si surface forming complexes which can be easily incorporated. Extended x-ray absorption fine-structure measurements have shown the existence of such complexes in Er-implanted Si, codoped with O.¹⁵ In addition, measurements of the 1.53 μ m photoluminescence performed for both samples in Fig. 3 show a distinctly different spectrum and luminescence lifetime, consistent with the fact that Er-O complexes have formed.¹⁶ Note that O also reduces Er segregation during Si SPE;^{6,7} indeed, the presence of O increases the effective solubility of Er in crystal Si.¹⁷

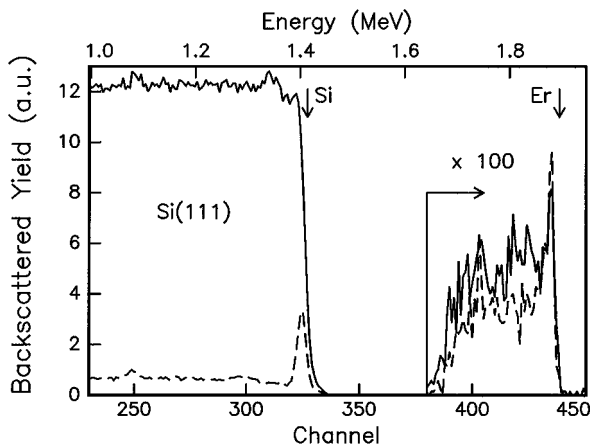


FIG. 4. RBS random (solid line) and channeling (dashed line) spectra for a MBE film grown on Si(111) at 600 °C. The Er flux was 3.1×10^{10} /cm² s. Channeling was performed in the [111] direction. The Er signal is magnified by a factor of 100. The arrows indicate the surface channels for Si and Er.

Er incorporation is very different during growth on Si(111). Figure 4 shows the RBS spectra taken in channeling and random conditions for a film grown on Si(111) under the same conditions as the film on Si(100) in Fig. 1. The channeling minimum yield for the film in the [111] direction shows a good epitaxial quality ($\chi_{\min} < 3\%$). From the figure it is apparent that for Si(111) without oxygen there is almost no Er segregation. The Er yield in the channeling spectrum is 29% lower than in the random spectrum. This indicates that this fraction of Er atoms is located in ordered positions relative to the [111] direction. We attribute this strong difference in the Er doping mode on Si(111) to the formation of epitaxial silicide precipitates. It is known that Er₃Si₅(0001) can be grown epitaxially on Si(111), with a lattice mismatch of only 1.22%.¹⁸

In conclusion, we have shown that strong Er segregation takes place during Si MBE with Er coevaporation on Si(100). Once a critical Er surface areal density of 2×10^{14} Er/cm² is achieved, an instability in the segregation/incorporation process takes place. The segregation can be completely suppressed by the presence of oxygen during deposition, possibly due to the formation of Er-O complexes. During MBE on Si(111) no Er segregation is observed, which is attributed to the growth of epitaxial erbium silicide precipitates.

We gratefully acknowledge discussions with H. A. van der Vegt. This work is part of the research program of FOM and was made possible by financial support from NWO, STW, and IOP Electro-Optics. R. Serna acknowledges financial support from CSIC, Spain.

- ¹ Y. H. Xie, E. A. Fitzgerald, and Y. J. Mii, *J. Appl. Phys.* **70**, 3223 (1991).
- ² H. Ennen, J. Schneider, G. Pomrenke, and A. Axmann, *Appl. Phys. Lett.* **43**, 943 (1983).
- ³ P. N. Favenec, H. L'Haridon, D. Moutonnet, M. Salvi, and M. Gauneau, *Jpn. J. Appl. Phys.* **29**, L521 (1990).
- ⁴ J. Michel, J. L. Benton, R. F. Ferrante, D. C. Jacobson, D. J. Eaglesham, E. A. Fitzgerald, Y.-H. Xie, J. M. Poate, and L. C. Kimerling, *J. Appl. Phys.* **70**, 2672 (1991).
- ⁵ A. Polman, J. S. Custer, E. Snoeks, and G. N. van den Hoven, *Appl. Phys. Lett.* **62**, 507 (1993).
- ⁶ J. S. Custer, A. Polman, and H. M. van Pinxteren, *J. Appl. Phys.* **75**, 2809 (1994).
- ⁷ F. Priolo, S. Coffa, G. Franzó, C. Spinella, A. Carnera, and V. Bellani, *J. Appl. Phys.* **74**, 4936 (1993).
- ⁸ H. Ennen, G. Pomrenke, A. Axmann, K. Eisele, W. Haydl, and J. Schneider, *Appl. Phys. Lett.* **46**, 381 (1985).
- ⁹ H. Efeogiu, J. H. Evans, J. M. Langert, A. R. Peaker, N. L. Rowel, J. P. Noel, D. D. Perovic, T. E. Jackman, and D. C. Houghton, *Mater. Res. Soc. Proc.* **220**, 367 (1991).
- ¹⁰ H. E. Efeogiu *et al.*, *Semicond. Sci. Technol.* **8**, 238 (1993).
- ¹¹ F. Arnaud D'Avitaya, Y. Campidelli, J. A. Chroboczek, P. N. Favenec, H. L'Haridon, D. Moutonnet, and A. Wasiela, *Mater. Res. Soc. Symp. Proc.* **301**, 97 (1993).
- ¹² S. Andrieu, F. Arnaud d'Avitaya, and J. C. Pfister, *J. Appl. Phys.* **65**, 2687 (1989).
- ¹³ S. Coffa, G. Franzó, F. Priolo, A. Polman, and R. Serna, *Phys. Rev. B* **49**, 16313 (1994).
- ¹⁴ S. Esch, M. Hohage, T. Michely, and G. Comsa, *Phys. Rev. Lett.* **72**, 518 (1994).
- ¹⁵ D. L. Adler, D. C. Jacobson, D. C. Eaglesham, M. A. Marcus, J. L. Benton, J. M. Poate, and P. H. Citrin, *Appl. Phys. Lett.* **61**, 2181 (1992).
- ¹⁶ R. Serna, J. H. Shin, A. Polman, M. Lohmeier, and E. Vlieg (unpublished).
- ¹⁷ A. Polman, G. N. van de Hoven, J. S. Custer, J. H. Shin, R. Serna, and P. F. A. Alkemade, *J. Appl. Phys.* **77**, 1256 (1995).
- ¹⁸ J. A. Knapp and S. T. Picraux, *Appl. Phys. Lett.* **48**, 466 (1986).